Determination of the Ion Temperature in a High-Energy-Density Plasma Using the Stark Effect

Dror Alumot,[1,*] Eyal Kroupp,[1] Evgeny Stambulchik,[1,†] Alexander Starobinets,[1]
Ingo Uschmann,[2] and Yitzhak Maron[1]
[1]*Faculty of Physics, Weizmann Institute of Science, Rehovot 7610001, Israel*
[2]*Institut für Optik und Quantenelektronik, Friedrich-Schiller-Universität Jena, Max-Wien-Platz 1, D-07743 Jena, Germany*

(Received 2 July 2018; revised manuscript received 21 January 2019; published 6 March 2019)

We present the experimental determination of the ion temperature in a neon-puff Z pinch. The diagnostic method is based on the effect of ion coupling on the Stark line shapes. It was found, in a profoundly explicit way, that at stagnation the ion thermal energy is small compared to the imploding-plasma kinetic energy, where most of the latter is converted to hydromotion. The method here described can be applied to other highly nonuniform and transient high-energy-density plasmas.

DOI: 10.1103/PhysRevLett.122.095001

Introduction.—The conversion of the kinetic energy of accelerated plasmas to ion heating, resulting in radiation emission or in nuclear fusion, is of fundamental interest in the field of high-energy-density (HED) plasmas and has general implications for laboratory and astrophysical plasma research [1–6]. Of particular importance is the determination of the ion thermal energy, addressed here.

In a stationary plasma, the ion temperature is associated with the spread of the kinetic energy K_i per ion. The latter is manifested in the Doppler broadening of spectral lines emitted [7] or, in the case of fusion plasmas, in a respective spread of the energy spectra of neutrons and other products of the fusion reactions [8–11]. However, for plasmas formed in the process of implosions, that is, in Z pinches and inertial confinement fusion (ICF) experiments, both thermal *and* hydrodynamic motions contribute to K_i. Therefore, the *apparent* ion Doppler "pseudotemperature" $T_i^D = \frac{2}{3}\langle K_i \rangle$ may be a significant overestimation of the *true* ion temperature T_i. Indeed, it was shown [12] that the ion temperature at stagnation—a culmination of the plasma implosion—may be an order of magnitude lower than T_i^D [13], with the rest of the kinetic energy likely stored in an ultrasonic turbulence [14]. However, even smaller differences between T_i^D and T_i are crucial for the fusion processes, whose rates depend drastically on T_i, while the residual kinetic energy [15] (hydromotion) is irrelevant. Furthermore, in an imploding plasma the electron temperature T_e [16] cannot be assumed to represent T_i, either: The radial kinetic energy is first transferred to T_i and then to T_e. Thus, $T_e < T_i < T_i^D$ until fully thermalized (which happens at late times, irrelevant for ICF).

The great challenge of determining the true T_i was solved in a previous study [12] by performing a detailed energy balance on a specific region of the plasma, relying on measuring the *entire history* of $\langle K_i \rangle$ and many other parameters of the plasma in this region *and* around it. However, such extensive diagnostics and analysis are rarely feasible. Contrary to that, here we present direct measurements of the ion temperature in a HED plasma that avoid the energy-balance complexities by using a different approach, requiring only *localized instantaneous* spectroscopic data. The underlying physical phenomenon is the ion-temperature dependence of the Stark profile of certain lines in moderately coupled plasmas.

We demonstrate this approach by measuring T_i at the stagnation phase of a neon-puff Z pinch, where, similar to the ICF implosions, the $T_e < T_i < T_i^D$ inequality holds [12]. Z pinch is a pulsed-current system widely used [17] for studying plasma implosions and for producing HED plasmas. In this system, an intense azimuthal magnetic field B_θ, induced by an axial current J_z, radially collapses a preconfigured load. The load, imploding under the $\vec{J} \times \vec{B}$ force, stagnates near the pinch axis, where a hot-and-dense plasma is formed for a few nanoseconds. The stagnation phase in similar Z-pinch devices studied earlier [12,13,18] is characterized by the electron density and temperature of $\lesssim 10^{21}$ cm^{-3} and $\sim$200 eV, respectively. These parameters are also typical for the measurements described here. Line shapes of H- and He-like neon ions were used for the diagnostics.

Stark-broadening sensitivity to T_i.—Stark line broadening is widely used for plasma diagnostics [19]. The Stark width depends strongly on the plasma density (typically, between $\propto N_e^{2/3}$ and $\propto N_e$); this is true for broadening due to plasma electrons and ions alike. Contrary to that, the temperature dependence is rather weak and sometimes nonmonotonic. Furthermore, the electron and ion contributions may have opposite

tendencies, resulting in a nearly complete cancellation over a wide temperature range [20]. Consequently, the Stark diagnostics is typically perceived as synonymous to the density diagnostics. However, if N_e and T_e are known with a sufficient precision independently of the line-shape measurements (e.g., using the Thomson scattering [21] or dielectronic satellite ratios [22]), then even the moderate Stark-width sensitivity to T_i can be used to infer the latter; this approach is used in the present study.

The first members of spectroscopic series of hydrogenlike ions are affected by ion dynamics (see [23] and references therein) and, therefore, are sensitive to T_i [24]. However, in HED plasmas, the shapes of these lines are often dominated by the Doppler or opacity effects [7]. On the other hand, for lines that originate from levels with a sufficiently high principal quantum number n (for brevity, "high-n lines"), the ion dynamics is typically of little importance [25,26]. Indeed, the method employed here is based on a different phenomenon.

The static Stark effect in a hydrogenlike atom is proportional to the electric field F. In a plasma, the charged particles form a microfield distribution around the typical field value that depends on the density N_p and charge q_p of the plasma particles as $\propto |q_p| N_p^{2/3}$. This distribution is sufficient for evaluating the plasma broadening by the heavy plasma particles (ions) when their Stark effect can be described in the quasistatic approximation [19]. Furthermore, the electron broadening is usually smaller than that due to the ions because of the dynamical nature of the electron perturbation [19] and the larger ion charge ($|q_i/e| > 1$). Thus, the broadening of these lines is mainly determined by the ion microfield distribution.

In an ideal plasma, the microfield distribution is a universal Holtsmark function [27] that is independent of the temperature. However, Coulomb interactions between the particles modify [28] the Holtsmark distribution, due to the Debye screening and the repulsion between the ions and the positively charged radiators [which can be also expressed in terms of the ion radial distribution function $g(r)$ around the radiator], resulting in a decrease of the Stark broadening.

Figure 1 demonstrates this point, showing Ne X Ly-δ ($n = 5 \to n = 1$) and Ly-ε ($n = 6 \to n = 1$) Stark profiles calculated for fixed $N_e = 10^{21}$ cm^{-3} and $T_e = 250$ eV but assuming two different values of T_i. In the calculations, based on a variant [29] of the computer simulation modeling [30], all quantum states with $n \leq 7$ were included [31]. As is seen, the lower (equal to T_e) T_i results in noticeably narrower widths compared to those at the higher $T_i = 1000$ eV.

The Debye screening influences the ion fields at large distances ($r \gtrsim \lambda_{D,i}$, where $\lambda_{D,i}$ is the ion Debye length), while the Coulomb repulsion is important only at short distances ($r \lesssim r_{m,i}$, where $r_{m,i} = q_i^2/T_i$ is the classical distance of the minimal approach). In a weakly nonideal

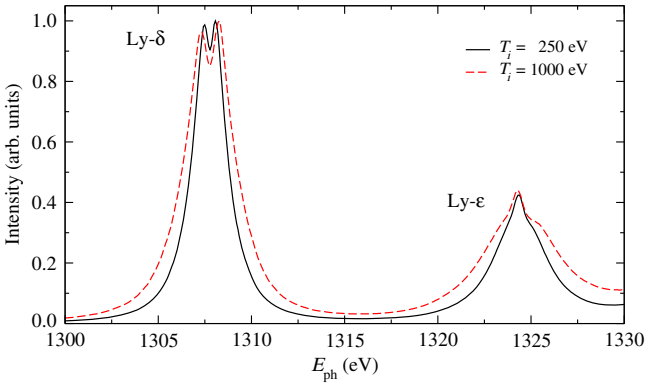

FIG. 1. Sensitivity of Stark broadening to the ion temperature. Results of computer simulations of the Ne X Lyman series in a neon plasma with $N_e = 10^{21}$ cm^{-3} and $T_e = 250$ eV are given (only shown is a spectral range containing Ly-δ and Ly-ε). The spectra are peak normalized.

plasma, the double inequality $r_{m,i} \ll r_i \ll \lambda_{D,i}$ holds, where $r_i = (4\pi N_i/3)^{-1/3}$ is a typical interion distance; since the linewidth is mostly affected by microfields formed by ions at distances $\sim r_i$, the ion-temperature corrections in such a plasma are minor, and the respective effect on the line broadening is small. However, the more nonideal the plasma is [characterized by the ion-ion coupling parameter $\Gamma_{ii} = q_i^2/(r_i T_i)$], the stronger the corrections become.

As an example, in Fig. 2 is shown the width of Ne X Ly-δ, calculated [32] as a function of Γ_{ii} for a few values of the electron density at a fixed electron temperature. Ly-ε displays similar features. It is seen that, for each density, there is a range of Γ_{ii} where the dependence of the Stark width on it and, hence, on the ion temperature can be used for the determination of T_i: For too high T_i (weakly coupled plasma) the Stark broadening is not sensitive to T_i, and for low T_i the Stark contribution becomes comparable to or even smaller than the Doppler width, especially for lower plasma densities.

Experimental setup.—Our Z-pinch generator (60 kV, 500-kA peak current, 500-ns rise time) implodes a neon-puff load in a 9-mm anode-cathode gap. The gas is injected into the gap through an annular nozzle (the cathode) that produces the outer gas cylinder and through an on-axis nozzle that produces the inner jet. Stagnation on axis of 10-ns duration is reached in ~500 ns.

The x-ray output from the stagnating plasma is recorded by a $\gtrsim$700-eV-filtered photoconductive detector (PCD). The spectroscopic system includes three spherical crystals, recording the neon Ly-α satellites and the high-n Ly-δ and Ly-ε, respectively. Each spectrometer allows for imaging the spectra along the Z-pinch axis with a spatial resolution of $\lesssim$50 μm. Two singly gated (~1 ns) intensified charge-coupled device cameras record the spectra collected by the spectrometers. The Ly-α satellite spectra are recorded with

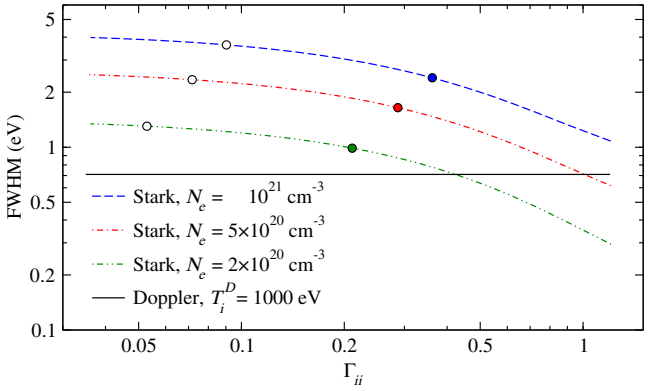

FIG. 2. Ne X Ly-δ Stark width as a function of Γ_{ii}, assuming three values of the electron density and a constant $T_e = 250$ eV. The filled and opaque circles correspond to $T_i = T_e = 250$ eV and $T_i = T_i^D = 1000$ eV, respectively. Also shown is the Doppler broadening.

a second-order spherical KAP crystal, yielding a resolving power of $\gtrsim$6700 with a Lorentzian-shaped spectral response. Combined with collisional-radiative (CR) modeling [33], the spectra provide the time-resolved electron density and the total (thermal and hydro) ion velocities at any z position [12,13]. Ly-δ and Ly-ε are recorded independently using two spherical fourth-order mica crystals, yielding resolving powers of $\gtrsim$5000 with a Lorentzian-shaped instrumental broadening.

Two singly gated multichannel plate (MCP) detectors are used, one for the Ly-α satellite spectra and the other for Ly-δ and Ly-ε. A high-voltage pulse generator is used to trigger both MCP detectors. With a delay correcting for the photon propagation, this allows for simultaneously recording all three spectra, imaged along z and integrated over the pinch chord. We note that, even though a single high-n line is sufficient for application of the method, two such lines (Ly-δ and Ly-ε) were recorded to decrease the uncertainties.

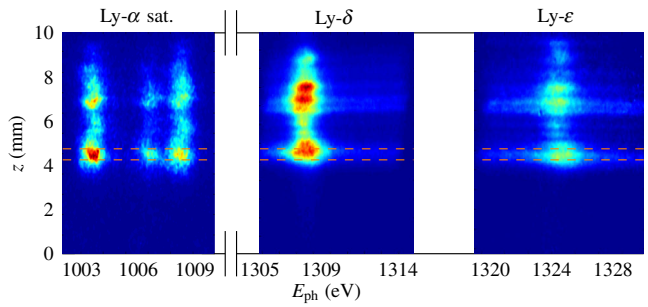

FIG. 3. Ly-α-satellites and high-n-line spectra recorded simultaneously at $t = 0$, axially resolved across the anode-cathode gap. The positions of the hot spots in all three spectra clearly match. The dashed lines highlight the slice from which the data are analyzed. The Ly-α and high-n spectra are normalized to the peak intensities of the Ly-α singlet satellite and Ly-δ, respectively.

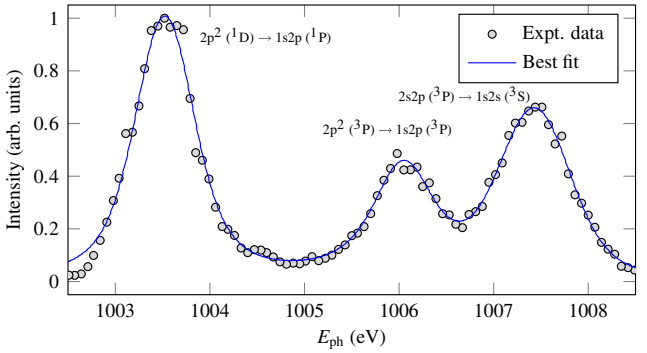

FIG. 4. Ne IX Ly-α satellite spectra: The experimental data are fit with three Voigt profiles. The Gaussian width of the singlet peak gives the total ion kinetic energy $T_i^D = 900 \pm 200$ eV, and the ratio between the integrated intensities of the two triplet groups gives the electron density $N_e = (6 \pm 1) \times 10^{20}$ cm^{-3} using the CR modeling.

See Supplemental Material [34] for more details on the experimental setup.

Results and discussion.—Typical spectra at the time of the peak PCD signal ($t = 0$) are shown in Fig. 3. In this example, analyzed are the z-averaged spectra from an axial slice $\Delta z = 0.5$ mm, centered at $z = 4.5$ mm ($z = 0$ corresponds to the cathode surface).

The shapes of the singlet and two triplet-satellite groups are fit with Voigt profiles. The shape of the singlet Ly-α satellite provides, after deconvolution of the instrumental spectral response, the total Doppler broadening (the Stark broadening is negligible for these lines, the natural widths are small, and the opacities are very low for the present parameters), as has been described [12,13]. For the example in Fig. 4, we obtain $T_i^D = 900 \pm 200$ eV. The triplet-to-singlet ratio of the integrated intensities of the satellite groups, together with CR modeling, is used to obtain the electron density in the plasma [12–14]. Accounting for the

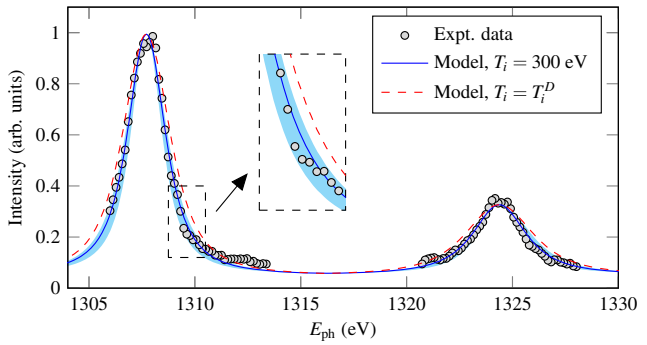

FIG. 5. The experimental high-n spectra are compared to line shape modeling for two values of T_i assumed: 300 eV and T_i^D. $T_i^D = 900$ eV, $N_e = 6 \times 10^{20}$ cm^{-3}, and $T_e = 200$ eV are assumed in both cases. The shaded area designates a spread of modeled spectra for T_i varying between 150 and 450 eV. An enlarged part of the graph is given in the inset.

TABLE I. The measured plasma parameters for various times throughout stagnation.

Shot No.	t (ns)	N_e (10^{20} cm^{-3})	T_i^D (eV)	T_i (eV)
WIZ2149	−2.5	5.0 ± 1.0	1900 ± 400	400 ± 150
WIZ2119	−1.5	3.0 ± 0.5	1100 ± 300	300 ± 150
WIZ1684	−1.0	3.5 ± 0.5	1300 ± 300	350 ± 150
WIZ1715	0.0	6.0 ± 1.0	900 ± 200	300 ± 150
WIZ1676	2.0	2.5 ± 0.5	1000 ± 250	550 ± 250
WIZ1673	2.5	5.5 ± 1.0	600 ± 200	400 ± 150
WIZ2138	4.0	2.5 ± 0.5	600 ± 200	550 ± 200

uncertainties in the experimental signals and in the atomic data used for the modeling, an effective [14] $N_e = (6 \pm 1) \times 10^{20}$ cm^{-3} is obtained.

The spectra of Ly-δ and Ly-ε were modeled by convolving the calculated Stark line shapes with the Doppler and instrumental broadenings. By varying T_i between zero and T_i^D, a best fit is obtained. T_e used in these calculations was determined to be 200 ± 30 eV based on the continuum slope [18] and agrees with the values assumed in similar studies [12,13]; the Stark line shapes depend negligibly on T_e within this range. Results of the high-n line shape analysis are presented in Fig. 5, demonstrating that the best fit is obtained for $T_i = 300 \pm 150$ eV, while assuming $T_i = T_i^D$ results in line shapes that are far from fitting the data [34].

The spectral analysis was performed on multiple shots at various times throughout stagnation. The results are summarized in Table I. We observe that most of the kinetic energy of the ions is stored not in the thermal motion but rather in a form of the hydrodynamic macromotion, while the true ion temperature is, as a rule, close to the electron temperature. These findings are in qualitative agreement with the previous results [12] that were based on energy-balance considerations.

Since the measurements are radially integrated, the inferred values are weighted-average ones, with the local emissivity being the weighting function. Interestingly, at $t = 2$ and 4 ns, the inferred T_i is rather high, closer to T_i^D, which can be an indirect manifestation of the turbulent motion. Indeed, it was noted [14] that a plasma similar to the one studied here is likely to be slightly nonisothermal. In a nonisothermal plasma, variations of the electron density and temperature are related through $T_e \propto N_e^{\gamma-1}$, where γ is the polytropic index ($\gamma = 1$ corresponds to isothermality). On the other hand, the intensity of the He-like satellites and that of H-like high-n lines depend differently on T_e; namely, the H-like line intensities rise with T_e significantly more strongly. Therefore, in the presence of turbulence-caused *positively correlated* fluctuations of N_e and T_e, the H-like Ly-δ and Ly-ε are on average emitted from higher-N_e regions than the He-like Ly-α satellites. Thus, N_e inferred from the Ly-α satellites is somewhat lower than the value required for calculating the Stark broadening of the H-like high-n lines. With N_e corrected, the Stark broadening would be larger, requiring a lower best-fit T_i to compensate (see Fig. 2). A deviation from the isothermality depends on the plasma density: The lower the density, the slower the thermal conduction [42]. Indeed, at $t = 2$ and 4 ns, the density was rather low. Notably, the stagnated plasma in the much larger Z machine [43] has typical parameters [6] that ensure isothermality to a very high degree.

We emphasize that this is the first study where the ion temperature of a HED plasma is directly obtained from instantaneous localized measurements, without the necessity to obtain an entire history of the plasma parameters and without relying on complex energy-balance argumentations. Thus, the approach described here may be considered for measurements in highly nonuniform and transient HED plasmas. The requirements for such measurements are (i) a moderate ion-ion coupling Γ_{ii}, (ii) the Stark broadening exceeding the Doppler one, and (iii) plasma with multiply ionized ions. If, as is often the case, tracers are used for diagnostics, instead of Γ_{ii}, one should use the radiator-ion coupling, $\Gamma_{ri} = q_r q_i/(r_i T_i)$ [29], where q_r is the charge of the radiator (tracer).

In Table II, we list typical plasma parameters and suggested tracer lines for determining T_i in selected prominent experiments. There, the Stark-to-Doppler width ratios w_S/w_D were calculated assuming $T_i^D = T_i$, evidently underestimating the Doppler broadening. However, the ratios are $\gg 1$, so that there is always a safe margin to ensure the Stark effect dominates the total linewidth. For given plasma conditions, the ratio can be adjusted either by using a higher-n (a stronger Stark effect) or a lower-energy transition (thus, reducing the Doppler broadening), e.g., a Balmer ($n \to n = 2$) instead of a Lyman transition.

TABLE II. Typical plasma parameters and a suggested tracer transition for the analysis in a few major experiments. Also given are the radiator–ion-perturber coupling Γ_{ri} and the ratio of the Stark to Doppler broadening w_S/w_D, with $T_i^D = T_i$ assumed for the latter.

Experiment	N_e (cm^{-3})	T_i (eV)	Plasma composition	$\lvert q_i/e \rvert$	Tracer line	Γ_{ri}	w_S/w_D
Radiating shock [5]	10^{22}	300	Plastic	3	Si Ly-γ	0.45	7
Capsule implosion [4]	2×10^{23}	3000	Plastic	3	Ar Ly-β	0.16	6
ICF hohlraum with dot tracers [44]	2×10^{21}	1000	Aluminum	13	Al Balmer-β	0.21	10
ICF gold bubble [45]	2×10^{21}	1000	Gold	50	Na Ly-ε	0.40	5

Evidently, spectral lines of other charge states (e.g., He-like) can also be considered. Thus, the freedom of choosing the transition and the tracer species itself provides sufficient flexibility for employing the diagnostic method described here in a variety of major HED experiments.

Finally, we note that the uncertainties in the inferred T_i are in part due to uncertainties in the line-shape calculations; this study is not unique in this respect. The Spectral Line Shapes in Plasma code comparison workshops [46] represent a major effort for assessing the accuracy of line-shape models. However, to the best of our knowledge, no benchmark experiments exist at HED plasma conditions. Therefore, we believe this should urge the community to carry out such measurements.

Fruitful discussions with A. Fisher and invaluable suggestions and reading the manuscript by O. L. Landen and M. B. Schneider are gratefully acknowledged. We thank P. Meiri for his skilled assistance, O. Wehrhan for preparing the mica crystals, and F. Schäfers and B. Marx for their help during the rocking curve measurements at BESSY-II. We are grateful to two anonymous referees for providing very valuable comments and suggestions. This work was supported in part by the Cornell Multi-University Center for High Energy-Density Science (USA), the Israel Science Foundation, and the Air Force Office of Scientific Research (USA).

*Corresponding author.
droralumot@gmail.com
Present address: Applied Materials, Rehovot, Israel.
†Corresponding author.
evgeny.stambulchik@weizmann.ac.il

[1] B. A. Remington, R. P. Drake, and D. D. Ryutov, Experimental astrophysics with high power lasers and z pinches, Rev. Mod. Phys. **78**, 755 (2006).

[2] M. Herrmann, A promising advance in nuclear fusion, Nature (London) **506**, 302 (2014).

[3] S. A. Slutz, M. C. Herrmann, R. A. Vesey, A. B. Sefkow, D. B. Sinars, D. C. Rovang, K. J. Peterson, and M. E. Cuneo, Pulsed-power-driven cylindrical liner implosions of laser preheated fuel magnetized with an axial field, Phys. Plasmas **17**, 056303 (2010); M. E. Cuneo *et al.*, Magnetically driven implosions for inertial confinement fusion at Sandia National Laboratories, IEEE Trans. Plasma Sci. **40**, 3222 (2012); S. A. Slutz *et al.*, Experimental Demonstration of Fusion-Relevant Conditions in Magnetized Liner Inertial Fusion, Phys. Rev. Lett. **113**, 155003 (2014).

[4] J. E. Bailey, G. A. Chandler, S. A. Slutz, I. Golovkin, P. W. Lake, J. J. MacFarlane, R. C. Mancini, T. J. Burris-Mog, G. Cooper, R. J. Leeper, T. A. Mehlhorn, T. C. Moore, T. J. Nash, D. S. Nielsen, C. L. Ruiz, D. G. Schroen, and W. A. Varnum, Hot Dense Capsule-Implosion Cores Produced by Z-pinch Dynamic Hohlraum Radiation, Phys. Rev. Lett. **92**, 085002 (2004).

[5] G. A. Rochau, J. E. Bailey, Y. Maron, G. A. Chandler, G. S. Dunham, D. V. Fisher, V. I. Fisher, R. W. Lemke, J. J. MacFarlane, K. J. Peterson, D. G. Schroen, S. A. Slutz, and E. Stambulchik, Radiating Shock Measurements in the Z-pinch Dynamic Hohlraum, Phys. Rev. Lett. **100**, 125004 (2008).

[6] Y. Maron, A. Starobinets, V. I. Fisher, E. Kroupp, D. Osin, A. Fisher, C. Deeney, C. A. Coverdale, P. D. Lepell, E. P. Yu, C. Jennings, M. E. Cuneo, M. C. Herrmann, J. L. Porter, T. A. Mehlhorn, and J. P. Apruzese, Pressure and Energy Balance of Stagnating Plasmas in z-Pinch Experiments: Implications to Current Flow at Stagnation, Phys. Rev. Lett. **111**, 035001 (2013).

[7] H. R. Griem, *Principles of Plasma Spectroscopy* (Cambridge University Press, Cambridge, England, 1997).

[8] B. Appelbe and J. Chittenden, The production spectrum in fusion plasmas, Plasma Phys. Controlled Fusion **53**, 045002 (2011).

[9] M. Gatu Johnson, D. T. Casey, J. A. Frenje, C.-K. Li, F. H. Séguin, R. D. Petrasso, R. Ashabranner, R. Bionta, S. LePape, M. McKernan, A. Mackinnon, J. D. Kilkenny, J. Knauer, and T. C. Sangster, Measurements of collective fuel velocities in deuterium-tritium exploding pusher and cryogenically layered deuterium-tritium implosions on the NIF, Phys. Plasmas **20**, 042707 (2013).

[10] T. J. Murphy, The effect of turbulent kinetic energy on inferred ion temperature from neutron spectra, Phys. Plasmas **21**, 072701 (2014).

[11] B. K. Spears, D. H. Munro, S. Sepke, J. Caggiano, D. Clark, R. Hatarik, A. Kritcher, D. Sayre, C. Yeamans, J. Knauer, T. Hilsabeck, and J. Kilkenny, Three-dimensional simulations of National Ignition Facility implosions: Insight into experimental observables, Phys. Plasmas **22**, 056317 (2015).

[12] E. Kroupp, D. Osin, A. Starobinets, V. Fisher, V. Bernshtam, L. Weingarten, Y. Maron, I. Uschmann, E. Förster, A. Fisher, M. E. Cuneo, C. Deeney, and J. L. Giuliani, Ion Temperature and Hydrodynamic-Energy Measurements in a z-pinch Plasma at Stagnation, Phys. Rev. Lett. **107**, 105001 (2011).

[13] E. Kroupp, D. Osin, A. Starobinets, V. Fisher, V. Bernshtam, Y. Maron, I. Uschmann, E. Förster, A. Fisher, and C. Deeney, Ion-Kinetic-Energy Measurements and Energy Balance in a Z-pinch Plasma at Stagnation, Phys. Rev. Lett. **98**, 115001 (2007).

[14] E. Kroupp, E. Stambulchik, A. Starobinets, D. Osin, V. I. Fisher, D. Alumot, Y. Maron, S. Davidovits, N. J. Fisch, and A. Fruchtman, Turbulent stagnation in a Z-pinch plasma, Phys. Rev. E **97**, 013202 (2018).

[15] A. L. Kritcher, R. Town, D. Bradley, D. Clark, B. Spears, O. Jones, S. Haan, P. T. Springer, J. Lindl, R. H. H. Scott, D. Callahan, M. J. Edwards, and O. L. Landen, Metrics for long wavelength asymmetries in inertial confinement fusion implosions on the National Ignition Facility, Phys. Plasmas **21**, 042708 (2014).

[16] L. C. Jarrott, B. Bachmann, T. Ma, L. R. Benedetti, F. E. Field, E. P. Hartouni, R. Hatarik, N. Izumi, S. F. Khan, O. L. Landen, S. R. Nagel, R. Nora, A. Pak, J. L. Peterson, M. B. Schneider, P. T. Springer, and P. K. Patel, Thermal Temperature Measurements of Inertial Fusion Implosions, Phys. Rev. Lett. **121**, 085001 (2018).

[17] D. D. Ryutov, M. S. Derzon, and M. K. Matzen, The physics of fast Z pinches, Rev. Mod. Phys. **72**, 167 (2000).

[18] D. Alumot, Determination of the Temperature and Density of Hot-Dense Plasma by Measuring the X-Ray Continuum Spectra, Master's thesis, Weizmann Institute of Science, 2007.
[19] H. R. Griem, *Spectral Line Broadening by Plasmas* (Academic, New York, 1974).
[20] E. Stambulchik and A. V. Demura, Dynamic Stark broadening of Lyman-α, J. Phys. B **49**, 035701 (2016).
[21] S. H. Glenzer and R. Redmer, X-ray Thomson scattering in high energy density plasmas, Rev. Mod. Phys. **81**, 1625 (2009).
[22] J. F. Seely, Density-Sensitive Dielectronic Satellite Lines in Microballon Neon Spectra, Phys. Rev. Lett. **42**, 1606 (1979).
[23] S. Ferri, A. Calisti, C. Mossé, J. Rosato, B. Talin, S. Alexiou, M. A. Gigosos, M. Á. González, D. González-Herrero, N. Lara, T. Gomez, C. A. Iglesias, S. Lorenzen, R. C. Mancini, and E. Stambulchik, Ion Dynamics Effect on Stark Broadened Line Shapes: A Cross Comparison of Various Models, Atoms **2**, 299 (2014).
[24] M. A. Gigosos, M. Á. González, and V. Cardeñoso, Computer simulated Balmer-alpha, -beta and -gamma Stark line profiles for non-equilibrium plasmas diagnostics, Spectrochim. Acta Part B **58**, 1489 (2003).
[25] E. Stambulchik, S. Alexiou, H. R. Griem, and P. C. Kepple, Stark broadening of high principal quantum number hydrogen Balmer lines in low-density laboratory plasmas, Phys. Rev. E **75**, 016401 (2007).
[26] S. Alexiou, E. Stambulchik, T. Gomez, and M. Koubiti, The fourth workshop on lineshape code comparison: Line merging, Atoms **6**, 13 (2018).
[27] J. Holtsmark, Über die Verbreiterung von Spektrallinien, Ann. Phys. (Berlin) **363**, 577 (1919).
[28] A. V. Demura, Physical models of plasma microfield, Int. J. Spectrosc. **2010**, 671073 (2010).
[29] E. Stambulchik and Y. Maron, A study of ion-dynamics and correlation effects for spectral line broadening in plasma: K-shell lines, J. Quant. Spectrosc. Radiat. Transfer **99**, 730 (2006).
[30] E. Stambulchik and Y. Maron, Plasma line broadening and computer simulations: A mini-review, High Energy Density Phys. **6**, 9 (2010).
[31] The interactions between the states with different n's result in a slight asymmetry of the line shapes. In addition, the "blue" wing of Ly-ϵ is affected by blending with the "red" wing of the Ly-ζ line ($n = 7 \rightarrow n = 1$, not shown in Fig. 1).
[32] E. Stambulchik and Y. Maron, Plasma formulary interactive, J. Instrum. **6**, P10009 (2011).
[33] Yu. V. Ralchenko and Y. Maron, Accelerated recombination due to resonant deexcitation of metastable states, J. Quant. Spectrsc. Radiat. Transfer **71**, 609 (2001).
[34] See Supplemental Material at http://link.aps.org/supplemental/10.1103/PhysRevLett.122.095001 for a discussion of the accuracy of the line-shape modeling, referring to studies [35–41].
[35] J. M. J. van Leeuwen, J. Groeneveld, and J. de Boer, New method for the calculation of the pair correlation function, Physica **25**, 792 (1959).
[36] C. A. Iglesias, J. L. Lebowitz, and D. MacGowan, Electric microfield distributions in strongly coupled plasmas, Phys. Rev. A **28**, 1667 (1983).
[37] A. Alastuey, C. A. Iglesias, J. L. Lebowitz, and D. Levesque, New systematic expansion of the electric field distribution in plasmas, Phys. Rev. A **30**, 2537 (1984).
[38] B. Held and P. Pignolet, Semi-empirical correlation function for one and two-ionic component plasmas, J. Phys. (Paris) **47**, 437 (1986).
[39] C. Iglesias, F. Rogers, R. Shepherd, A. Bar-Shalom, M. Murillo, D. Kilcrease, A. Calisti, and R. Lee, Fast electric microfield distribution calculations in extreme matter conditions, J. Quant. Spectrosc. Radiat. Transfer **65**, 303 (2000).
[40] E. Stambulchik, D. V. Fisher, Y. Maron, H. R. Griem, and S. Alexiou, Correlation effects and their influence on line broadening in plasmas: Application to H_α, High Energy Density Phys. **3**, 272 (2007).
[41] E. Stambulchik and Y. Maron, Quasicontiguous frequency-fluctuation model for calculation of hydrogen and hydrogenlike Stark-broadened line shapes in plasmas, Phys. Rev. E **87**, 053108 (2013).
[42] Ya. B. Zeldovich and Yu. Raizer, *Physics of Shock Waves and High-Temperature Hydrodynamic Phenomena* (Academic, New York, 1967).
[43] B. Jones, C. Deeney, C. Coverdale, P. LePell, J. McKenney, J. Apruzese, J. Thornhill, K. Whitney, R. Clark, A. Velikovich, J. Davis, Y. Maron, V. Kantsyrev, A. Safronova, and V. Oreshkin, K-shell radiation physics in low- to moderate-atomic-number z-pinch plasmas on the Z accelerator, J. Quant. Spectrosc. Radiat. Transfer **99**, 341 (2006).
[44] M. A. Barrios *et al.*, Experimental investigation of bright spots in broadband, gated x-ray images of ignition-scale implosions on the National Ignition Facility, Phys. Plasmas **20**, 072706 (2013); Heat transport modeling of the dot spectroscopy platform on NIF, Plasma Phys. Controlled Fusion **60**, 044009 (2018).
[45] M. B. Schneider, S. A. MacLaren, K. Widmann, N. B. Meezan, J. H. Hammer, B. E. Yoxall, P. M. Bell, D. K. Bradley, D. A. Callahan, M. J. Edwards, T. M. Guymer, D. E. Hinkel, W. W. Hsing, M. L. Kervin, O. L. Landen, J. D. Moody, A. S. Moore, N. E. Palmer, and A. T. Teruya, Images of the gold bubble feature in NIF gas-filled ignition hohlraums, J. Phys. Conf. Ser. **717**, 012049 (2016); H. Chen, N. Palmer, M. Dayton, A. Carpenter, M. B. Schneider, P. M. Bell, D. K. Bradley, L. D. Claus, L. Fang, T. Hilsabeck, M. Hohenberger, O. S. Jones, J. D. Kilkenny, M. W. Kimmel, G. Robertson, G. Rochau, M. O. Sanchez, J. W. Stahoviak, D. C. Trotter, and J. L. Porter, A high-speed two-frame, 1-2 ns gated X-ray CMOS imager used as a hohlraum diagnostic on the National Ignition Facility, Rev. Sci. Instrum. **87**, 11E203 (2016).
[46] Spectral Line Shapes in Plasmas workshops, http://plasma-gate.weizmann.ac.il/slsp/.